Journal of Integrative Neuroscience

J. Integr. Neurosci. **2025**; 24(10): 33497
https://doi.org/10.31083/JIN33497

Original Research

Rubiadin Alleviates Alzheimer's Disease Pathology via NF-κB Pathway Regulation

Ying Zhang[1], Jia Fan[1], Shanji Nan[1], Jiaqi Pan[1], Wanxu Guo[2], Yizhi Zhang[1,*]

[1]Department of Neurology, The Second Hospital of Jilin University, 130041 Changchun, Jilin, China
[2]Department of Neonatology, The Second Hospital of Jilin University, 130041 Changchun, Jilin, China
*Correspondence: yzzhang@jlu.edu.cn (Yizhi Zhang)

Academic Editor: Ulises Gomez-Pinedo
Submitted: 4 December 2024 Revised: 4 May 2025 Accepted: 28 May 2025 Published: 31 October 2025

Abstract

Background: Alzheimer's disease (AD) is a severe neurodegenerative disorder that impacts the global impact on the population. Nevertheless, the intricate nature of its pathogenesis has posed significant challenges to drug discovery in this field. This study aimed to verify the therapeutic potential of rubiadin (RB) on AD through both *in vivo* and *in vitro* experiments, thereby facilitating translational research for the advancement of AD treatment. **Methods**: We investigated the neuroprotective effects of RB on AD using both *in vivo* and *in vitro* models. Immunohistochemistry and western blot analysis were employed to evaluate inflammatory factors and the Nuclear Factor kappa-light-chain-enhancer of activated B cells (NF-κB) pathway in Mo/HuAPP695swe (APP)/PS1-dE9 (PS1) mice and N2a cells. **Results**: RB enhanced the memory performance of APP/PS1 mice in various tests, including the Morris water maze, step-down and step-through passive avoidance tasks, and novel object recognition. RB reduced the accumulation of Amyloid-beta (Aβ) plaques, as shown by immunohistochemical analysis. It also decreased the expression levels of pro-inflammatory cytokines interleukin (IL)-1β, IL-6, and tumor necrosis factor-alpha (TNF-α), while increasing the release of IL-4. Additionally, RB inhibited the NF-κB pathway, as demonstrated by western blot. Moreover, a cell viability test showed that RB protected N2a cells against toxicity caused by A$\beta_{1–42}$ through a cell viability test. Western blot analysis revealed that neuroinflammation and the NF-κB pathway were inhibited by RB treatment in A$\beta_{1–42}$-induced N2a cells. Accordingly, RB suppressed the nuclear translocation of NF-κB in A$\beta_{1–42}$-induced N2a cells. **Conclusions**: Our results provide experimental evidence supporting the preclinical research and future clinical applications of RB, thereby facilitating the development of new drugs for AD clinical therapy.

Keywords: rubiadin; Alzheimer's disease; neuroinflammation; NF-κB pathway

1. Introduction

Alzheimer's disease (AD) is a typical form of dementia familiar to the public for which aging is the primary risk factor. Longer life expectancies increase the risk of people suffering from AD [1]. Alzheimer's patients typically encounter memory deficits and reduced cognitive abilities alongside other complications, with the chronic nature of their condition creating escalating burdens for family systems and society at large [2]. Hence, the development of efficient therapies for AD has become a pressing necessity. Pathologically, AD is distinguished from other forms of dementia by the appearance of Amyloid-beta (Aβ) plaques and neurofibrillary tangles (NFTs) [3], which are considered the cornerstone of its pathogenesis. Despite the approval of lecanemab, a new monoclonal antibody that targets Aβ elimination, by the Food and Drug Administration earlier this year [4], advancements in drug development focused on Aβ and NFTs have continued to progress at a sluggish pace over recent decades [5]. Therefore, other important factors are also involved in AD progression.

The central role of glial cell-driven neuroinflammation in Alzheimer's pathogenesis is gaining growing recognition. A positron emission tomography (PET) imaging study has demonstrated that neuroinflammatory processes initiate at preclinical stages, preceding Aβ plaque deposition—a finding replicated in multiple transgenic rodent models [6]. Longitudinal observations reveal sustained activation of microglial cells in AD-affected brains [7]. A systematic review documented altered expression of inflammatory biomarkers in both central nervous system (CNS) and peripheral compartments, corroborating the systemic inflammatory phenotype of AD [8]. Mechanistically, Aβ accumulation promotes neuroinflammatory responses marked by cytokine secretion and activation of canonical signaling pathways including nuclear factor kappa-light-chain-enhancer of activated B cells (NF-κB) and mitogen-activated protein kinase (MAPK) [9]. Moreover, the heightened neuroinflammation fosters the production of additional Aβ plaques, leading to a vicious circle [10]. Neflamapimod, a selective inhibitor of p38 MAPK pathway, was confirmed to dampen biomarkers of synaptic impairment in the cerebrospinal fluid in a phase 2 clinical trial, which deserves further clinical trials before its application [11]. Thus, focusing on neuroinflammation may offer a potential pathway for the creation of therapeutic agents to tackle AD.

Due to their abundant sources and excellent safety profile, natural products and their derivatives have garnered increasing attention in the field of drug development [12]. In addition, their diverse and complex chemical structures may be sued to develop multi-target drugs [13]. For example, ferulic acid protected the hippocampal capillaries, lessened Aβ aggregation, and improved memory deficits in Mo/HuAPP695swe (APP)/PS1-dE9 (PS1) mice [14], which also regulated oxidative stress and inflammation. Rubiadin (RB) is an anthraquinone compound that mainly originates from the root of Rubia cordifolia Linn., an ancient medicinal plant found in Ayurveda [15]. RB has been documented to exhibit a broad spectrum of pharmacological activities, such as anticancer, anti-osteoporotic, hepatoprotective, antidiabetic, antioxidant, antifungal, and anti-inflammatory effects [16]. In particular, 500 mg of the RB suspension improved epileptic seizures caused by maximal electric shock and pentylene tetrazole, indicating its neuroprotective effects. However, no studies have explored whether RB plays a neuroprotective role in AD-related rodent or cell models.

This study systematically evaluated the neuroprotective efficacy of RB in Alzheimer's disease using transgenic APP/PS1 mice and Aβ_{1-42}-challenged N2a cells. Behavioral assessments including Morris water maze (MWM), step-down/step-through passive avoidance tasks, and novel object recognition (NOR) were employed to characterize memory improvement following RB administration. Amyloid plaque burden in APP/PS1 mouse brains was quantified via immunohistochemical staining, while inflammatory marker expression was analyzed using western blot techniques. To validate *in vitro* neuroprotection, an Aβ_{1-42}-exposed N2a cell model was established, with cytoprotective effects evaluated through cell viability assays, western blot analysis, and immunofluorescence microscopy. Collectively, these findings contribute preclinical evidence supporting RB's therapeutic potential and facilitate translational research toward AD treatment development.

2. Materials and Methods

2.1 Animals

Twenty APP/PS1 mice (8-month-old, 44–50 g) and ten wild-type (WT) littermate mice (8-month-old, 38–44 g) were provided by Liaoning Changsheng Biotechnology Co., Ltd. (Benxi, Liaoning, China). All mice stayed in the SPF-level laboratory, where each mouse lived in a single cage with sufficient water and food. 10 WT mice were included in the WT group (n = 10). All APP/PS1 mice were randomly and equally divided into the APP/PS1 group and RB-treated APP/PS1 group (n = 10). Mice in the WT and APP/PS1 group were given normal saline (0.9%) orally every day, while the RB-treated APP/PS1 mice were treated with 20 mg/kg RB (117-02-2, Chengdu Herbpurify Co., Ltd., Chengdu, Sichuan, China) through the same way. The intragastric administration dose was 0.1 mL/10 g, which means 0.1 mL was given for every 10 g of mouse body weight. The whole agent treatment lasted for 8 weeks and behavioral tests began since the 6th week. Subsequently, the mice were intraperitoneally injected with 150 mg/kg of pentobarbital (P3761, Sigma-Aldrich, Shanghai, China) sodium and their brain samples were procured for subsequent experimental analysis. Animal experiments were approved by Institutional Animal Care, use Committee of Jilin University (SY202103007), and the date (10-03-2021) of this approval. All procedures were in accordance with ARRIVE guidelines.

2.2 MWM Test

The MWM test was conducted on the 36th day. MWM test included 2 parts, the 6-day navigation test and 1-day probe trial. In the navigation test, mice were put into the muddy water containing TiO_2 in the tank which is 120 cm in diameter. Their goal was to find the platform, which was hidden 2 cm below the water surface, within a 60 s time limit. If they were unsuccessful in finding the platform, they would be guided to it and required to stay there for 30 s to become familiar with its location. All mice were trained for 5 days and the formal test was carried out on the 6th day (day 41st since the beginning of agent treatment). In the probe trial, the platform was taken away, and the mice were permitted to swim freely in the opaque water for 60 s. A video tracking system (XR-XM101, Shanghai XinRuan Information Technology Co., Ltd., Shanghai, China) was utilized to record the every-day escape latency, the crossing numbers in the platform area and time staying in this area in the probe trail, and their trajectories. Data analysis was conducted by an observer unaware of the treatment conditions.

2.3 Step-Down and Step-Through Passive Avoidance Test

Since the 44th day, the step-down test was initiated. The equipment consisted of was a square box (30 cm $\times$ 30 cm $\times$ 30 cm), with a circular platform (8 cm in diameter) positioned at its center (XR-3TB, Shanghai XinRuan Information Technology Co., Ltd., Shanghai, China). This platform was elevated 4 cm above a grid floor made of stainless steel. As previously mentioned, the mice were initially placed on the grid floor and subjected to an electric shock, prompting them to jump onto the platform to evade the stimulus. Following a 24-hour interval, the mice were placed on the platform again. The step-down latency was determined by measuring the time it took for each mouse to jump back down to the floor for the first time. A maximum step-through latency of 300 s was established. During this period, the number of times each mouse jumped down was recorded as error counts.

The step-through test [17] was performed since day 47th. The apparatus comprised two identical compartments (each measuring 20 cm $\times$ 13 cm $\times$ 12 cm), one illuminated and the other dark (XR-Med, Shanghai XinRuan Informa-

tion Technology Co., Ltd.). An automated doorway separated these two compartments. The floor in the dark compartment was charged with electricity. In the training session, the mice were first put in the light compartment for 10 s of free exploration. Later, the door was opened, and driven by their natural curiosity, the mice were inclined to enter the dark compartment. Upon chamber entry, the door was shut, and subjects received a 0.2 mA electric foot shock for 5 seconds. After a 48-hour interval, mice were placed back into the light compartment with the open-door configuration. The latency to enter the dark compartment was measured as step-through latency, with a 300-second ceiling. Blinded evaluation was conducted by an observer unaware of treatment assignments.

2.4 NOR Test

On day 50th, NOR test was performed referring to Wan *et al*. [18]. Initially, the mice were permitted to explore an empty apparatus (50 cm $\times$ 50 cm) for a period of 5 min to become accustomed to the environment. Subsequently, two identical objects, labeled A and B, were introduced into the apparatus, and the mice were given an additional 5 min to explore. Following the exploration phase, the mice were taken out, and the apparatus was meticulously cleaned with 75% ethyl alcohol to remove any remaining odors. Then, object B was substituted with a new object C, which was identical in size and material but featured a distinct shape. The time spent by the mice exploring each object was meticulously recorded by a video tracking system (XR-XM101). The recognition index (%) was calculated using the formula: New object exploration time / (new object exploration time + old object exploration time) $\times$ 100%. Data analysis was carried out by an observer unaware of the treatment groups to maintain objectivity.

2.5 Immunohistochemistry (IHC) Analysis

The general health status of the mice was closely monitored throughout the entire experimental period. Following the completion of behavioral tests, all mice were euthanized using CO_2 anesthesia. CO_2 was displaced into the euthanasia vessel at a flow rate of 40% of the chamber's volume per minute. Like Wan *et al*. [18], after mice were euthanized, the intact brain samples were fixed with 4% paraformaldehyde (BL539A, biosharp, Hefei, Anhui, China) instantly followed by dehydration and embedding. The paraffin-embedded blocks were cut into slices with a thickness of 5 µm. After re-hydrated, slices were subjected to antigen retrieval at 96 °C. Then slices were sequentially blocked with 5% bull serum albumin (abs9157, Absin (Shanghai) Bioscience Inc., Ltd., Shanghai, China), incubated with anti-Aβ_{1-42} (A24422, 1:500, ABclonal, Wuhan, China) and secondary antibody (E-AB-1003, 1:5000, Elabscience, Wuhan, Hubei, China), and finally stained with DAB and hematoxylin. All agents were from IHC detection kit (RK05872, ABclonal). Images were taken using microscope (BX51, Olympus, Beijing, China). For all antibodies' information see **Supplementary Material-antibodies**.

2.6 Cell Culture and Agent Treatment

N2a cells are a neuroblastoma cell line with neuronal and amoeboid stem cell morphology isolated from brain tissue. Mouse neuroblastoma N2a cells (CL-0168, Procell, Wuhan, Hubei, China) were maintained in MEM medium (11575032) supplemented with 10% fetal bovine serum (16140071) and 1% penicillin-streptomycin solution (15140148). Cells were cultured at 37 °C in a moist environment with 5% CO_2. All reagents were offered by Thermo (Waltham, MA, USA). The N2a cells used in the experiment were morphologically characterized and confirmed to be free of mycoplasma contamination.

For the agent treatment in the following experiments, in the 3 h pretreatment period, N2a cells in the RB-treated groups were treated with 5 µM RB and 20 µM RB, respectively. In both the control and model groups, the medium was replaced with an equal volume of basic MEM. Then in the 24 h treatment period, the control group was still treated with basic MEM. The model group was treated with 5 µM Aβ_{1-42} (107P64, Taigu Biology, Nanjing, Jiangsu, China). The RB-treated groups were firstly stimulated with 5 µM Aβ_{1-42}, then treated with 5 µM RB and 20 µM RB, respectively.

2.7 Cell Viability Test

This part refers to the previous method [19]. 100 µL of N2a cell suspension were added in the 96-well plate (5 $\times$ 10^4/mL) for cell viability test. Following the pretreatment for 3 h and treatment for 24 h as described in the "Cell Culture and Agent Treatment" section, 20 µL of a 5 mg/kg MTT (1334GR001, Guangzhou saiquo biotech Co., Ltd., Guangzhou, Guangdong, China) solution was added to the cells. Following incubation at 37 °C for 4 hours. The crystals were dissolved using dimethyl sulfoxide (D670381, Aladdin, Shanghai, China) and the absorbance was measured at 490 nm using microplate reader (Synergy 4, Omega Biotek, Inc., Norcross, GA, USA).

2.8 Cell Immunofluorescence

N2a cells were plated at 5 $\times$ 10^4 cells/mL on glass coverslips to evaluate nuclear translocation of NF-κB following RB treatment. After completing the pre-treatment and drug administration protocols described in section 2.6, culture medium was aspirated, and cells were washed with phosphate buffer. Sample preparation followed the manufacturer's instructions (SN368, Beyotime, Beijing, China). The slides were incubated with NF-κB (A2547, 1:300, ABclonal) antibodies, followed by secondary antibody (AS058, 1:500, ABclonal), and ultimately with DAPI (D1306, Thermofisher, Waltham, MA, USA). Confocal imaging was performed using a Zeiss LSM710 laser scanning microscope (Shanghai, China). For all antibodies' information see **Supplementary Material-antibodies**.

2.9 Western Blot

Brain sample were collected to homogenize (50 Hz, 60 s, twice) and centrifuge (13,000 rpm, 5 min, twice) to extract protein solution. After treatment was finished as shown in 2.6, N2a cells were collected to lyse (20 min) and centrifuge (13,000 rpm, 5 min, twice) to extract protein sample. The whole process of protein extraction was done under 4 °C. The solution was qualified using BCA kit (P0012S, beyotime, Shanghai, China). Proteins (30–40 µg) were separated using sodium dodecyl sulfate polyacrylamide gel electrophoresis (SDS-PAGE) and then transferred to PVDF membranes. Primary antibodies anti-IL-1β (A16288, 1:1000, ABclonal), anti-IL-4 (A14660, 1:1000, ABclonal), anti-IL-6 (A0286, 1:1000, ABclonal), anti-TNF-α (A11534, 1:1000, ABclonal), anti-p-inhibitor of kappa B kinase (IKK) (AP0546, 1:1000, ABclonal), anti-IKK (A2062, 1:3000, ABclonal), anti-p-inhibitor of NF-κB (IκB) (AP0614, 1:500, ABclonal), anti-IκB (A11397, 1:1000, ABclonal), anti-p-nuclear factor kappa-B (NF-κB) (AP0123, 1:400, ABclonal), anti-NF-κB (A2547, 1:1000, ABclonal), anti-p-Tau (bs-2392R, 1:2000, Bioss, Beijing, China) and anti-GAPDH (A19056, 1:5000, ABclonal) were used to incubate membranes at 4 °C overnight. The membranes were subsequently washed and incubated with goat anti-rabbit immunoglobulin G (IgG) (AS058, 1:10,000, ABclonal) at 4 °C for 4 hours. After incubation, membranes were washed again and analyzed by gel imager (GenoSens 2150, Beijing, China). For all antibodies' information see **Supplementary Material-antibodies**.

2.10 Statistical Analysis

Semi-quantitative analysis of immunohistochemical staining and western blot results was performed using ImageJ software (1.8.0.345, Bethesda, MD, USA). GraphPad Prism 9 (GraphPad Software, Inc., San Diego, CA, USA) was utilized to generate bar charts. Statistical comparisons among WT, APP/PS1, and RB-treated APP/PS1 groups were conducted with BONC DSS Statistics 25 software (Business-intelligence of Oriental Nations Co., Ltd., Beijing, China), presenting data as mean ± (standard error of the mean) SEM. The normality of the behavioral data was assessed using the Shapiro-Wilk test, and non-parametric statistical analysis was conducted via the Kruskal-Wallis H test due to potential deviations from normal distribution. For the comparison of multiple groups in the other data, one-way ANOVA was performed, followed by Least Significant Difference (LSD) post hoc analysis. Statistical significance was determined at $p < 0.05$. For original data see **Supplementary Material-Original data**.

3. Results

3.1 RB Ameliorated Memory Loss and Learning Ability of APP/PS1 Mice

MWM is widely utilized to evaluate spatial memory and learning capacities in rodent models [20]. Representative swimming trajectories on day 6 are presented in Fig. 1A. During the initial navigation session, no significant differences in platform localization time were observed among WT, APP/PS1, and APP/PS1 + RB groups (Fig. 1B). Following repeated training, RB-treated APP/PS1 mice demonstrated reduced search times compared to untreated counterparts (Fig. 1B). Notably, APP/PS1 mice displayed more disorganized swimming patterns compared to RB-treated animals. Statistical analysis revealed that RB administration significantly decreased escape latency during formal navigation testing in APP/PS1 mice ($p < 0.01$) (Fig. 1C). Probe trial results showed distinct trajectory patterns (Fig. 1D), with APP/PS1 mice spending significantly less time in the target quadrant compared to WT controls ($p < 0.01$) (Fig. 1E). Additionally, platform crossings were reduced in APP/PS1 mice ($p < 0.001$) (Fig. 1F). Significantly, RB intervention enhanced both target area occupancy and platform crossing frequency in APP/PS1 mice ($p < 0.05$, Fig. 1E,F). Passive avoidance testing (step-down/step-through) evaluated memory function following RB administration. Step-down test results showed APP/PS1 mice had shorter latency to step down compared to WT controls ($p < 0.001$, Fig. 1G). Additionally, APP/PS1 mice made more jump-down attempts within 5 minutes despite repeated shocks ($p < 0.001$, Fig. 1H). RB treatment reversed these impairments in APP/PS1 mice, increasing step-down latency ($p < 0.001$, Fig. 1G) and reducing jump-down frequency ($p < 0.01$, Fig. 1H). Step-through test results revealed RB-treated mice had significantly longer latency to enter the dark compartment compared to untreated APP/PS1 mice ($p < 0.001$, Fig. 1I). NOR test results showed APP/PS1 mice had impaired non-spatial recognition memory, reflected by reduced recognition index, which was improved by RB treatment ($p < 0.05$, Fig. 1J). These data indicate RB improves both spatial and non-spatial memory in APP/PS1 mice.

3.2 RB Decreased Cerebral Aβ Deposition and Neuroinflammation of APP/PS1 Mice

To investigate the pathological effects of RB treatment in APP/PS1 mice, immunohistochemical staining was performed to assess Aβ plaque distribution in cortical and hippocampal areas. Fig. 2 demonstrates that WT mice had almost no Aβ plaques, whereas APP/PS1 mice exhibited substantial Aβ accumulation in these regions ($p < 0.01$). Strikingly, RB-treated APP/PS1 mice showed significant reductions in Aβ plaque formation in both the cortex and hippocampus ($p < 0.05$, Fig. 2A–C).

Subsequently, western blot analysis was performed to assess inflammatory markers in APP/PS1 mouse brains. Compared to WT mice, APP/PS1 mice showed increased pro-inflammatory cytokines (IL-1β, IL-6, TNF-α) and decreased anti-inflammatory cytokine IL-4 ($p < 0.001$, Fig. 3A–E). RB treatment significantly reversed these alterations, reducing pro-inflammatory markers and increas-

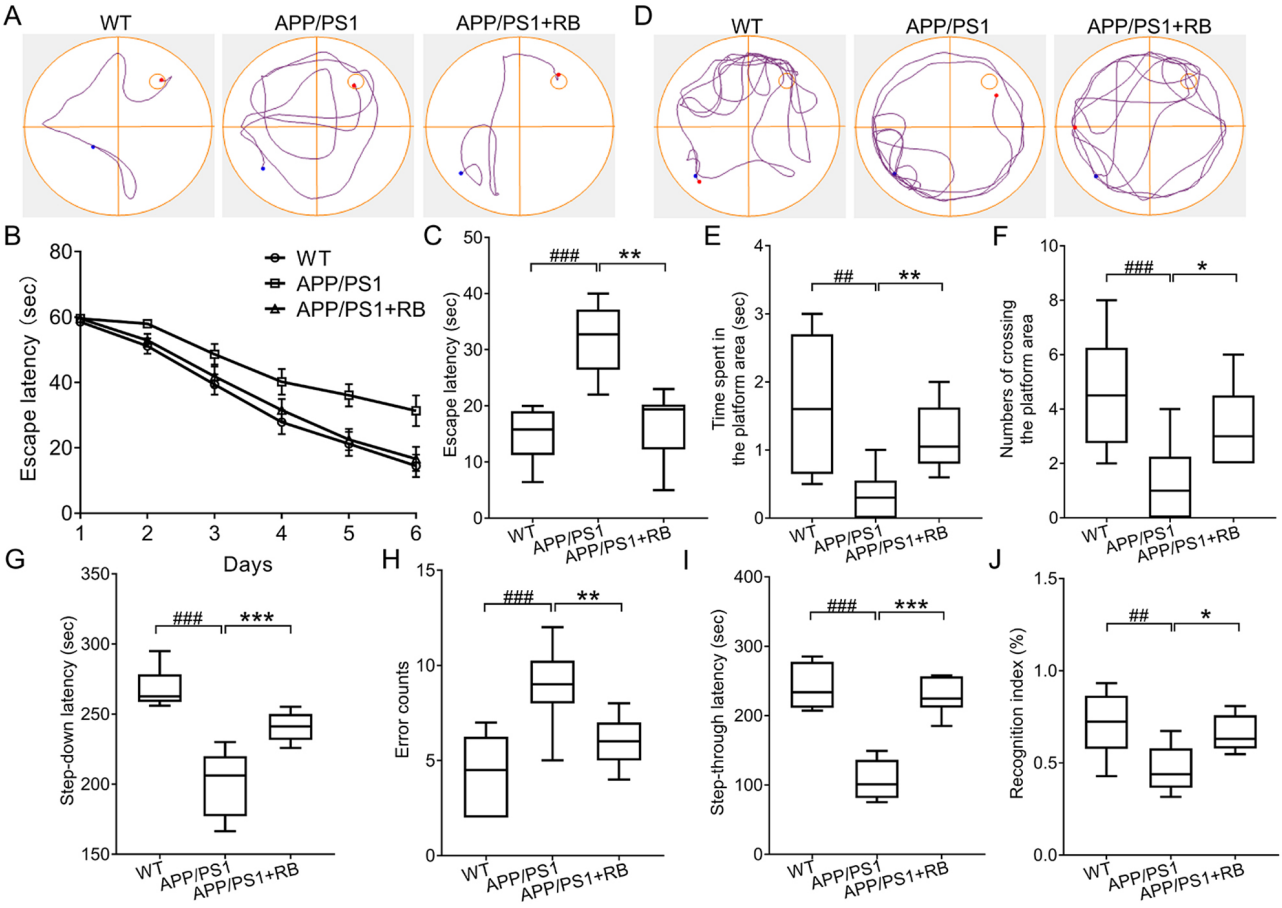

Fig. 1. RB ameliorated memory loss and learning ability of APP/PS1 mice. (A) Represent trajectories on day 6 in the navigation test (n = 10). The escape latency (B) from day 1 to day 6 and (C) on day 6 in the navigation part of MWM test (n = 10). (D) Represent trajectories of mice in the probe trial (n = 10). RB increased (E) time that mice spent in the platform area and (F) numbers of crossing the platform area (n = 10). (G,H) RB improved the memory performance of APP/PS1 mice in the step-down passive avoidance test (n = 10). (I) RB extended the step-through latency of APP/PS1 mice in the step-through passive avoidance test (n = 10). (J) RB enhanced the recognition index of APP/PS1 mice in the NOR test (n = 10). $^{\#\#}p < 0.01$, $^{\#\#\#}p < 0.001$ compared with WT mice; $^{*}p < 0.05$, $^{**}p < 0.01$, and $^{***}p < 0.001$ compared with APP/PS1 mice. RB, rubiadin; APP/PS1, Mo/HuAPP695swe/PS1-dE9; MWM, Morris water maze; NOR, novel object recognition; WT, wild-type.

ing IL-4 levels ($p < 0.05$, Fig. 3A–E), confirming its anti-inflammatory properties. Phosphorylation of NF-κB signaling components was also evaluated. RB treatment significantly suppressed phosphorylation of IKK, IκB, and NF-κB in APP/PS1 mice compared to untreated controls ($p < 0.001$, Fig. 3F–I), further supporting its role in mitigating neuroinflammation. For all original WB figures in Fig. 3A,F, see the **Supplementary Material-original images of WB**.

3.3 RB Protected N2a Cells Against Aβ_{1-42}-Induced Cell Damage and Inflammation

To further validate RB's neuroprotective effects *in vitro*, N2a cells were challenged with Aβ_{1-42}. RB treatment significantly improved cell viability in Aβ_{1-42}-exposed N2a cells ($p < 0.001$, Fig. 4A), indicating its cytoprotective potential. Compared to control cells, Aβ_{1-42} exposure induced marked increases in pro-inflammatory cytokines (IL-1β, IL-6, TNF-α) and decreases in anti-inflammatory IL-4 ($p < 0.01$, Fig. 4B–F), reflecting inflammatory activation. For all original WB figures in Fig. 4B, see the **Supplementary Material-original images of WB**. Concurrently, Aβ_{1-42} treatment significantly upregulated phosphorylated Tau protein expression in N2a cells ($p < 0.001$, Fig. 4G). RB administration effectively restored cytokine balance and reduced p-Tau levels in Aβ_{1-42}-treated cells ($p < 0.01$, Fig. 4B–G), demonstrating its inhibitory effects on inflammatory responses.

3.4 RB Blunted the Activation of IKK/IκB/NF-κB Pathway

To further confirm whether NF-κB was regulated in Aβ_{1-42}-treated N2a cells, the phosphorylation of NF-κB and its upstream IKK and IκB was detected through western blot. Once the N2a cells were treated with 5 µM Aβ_{1-42},

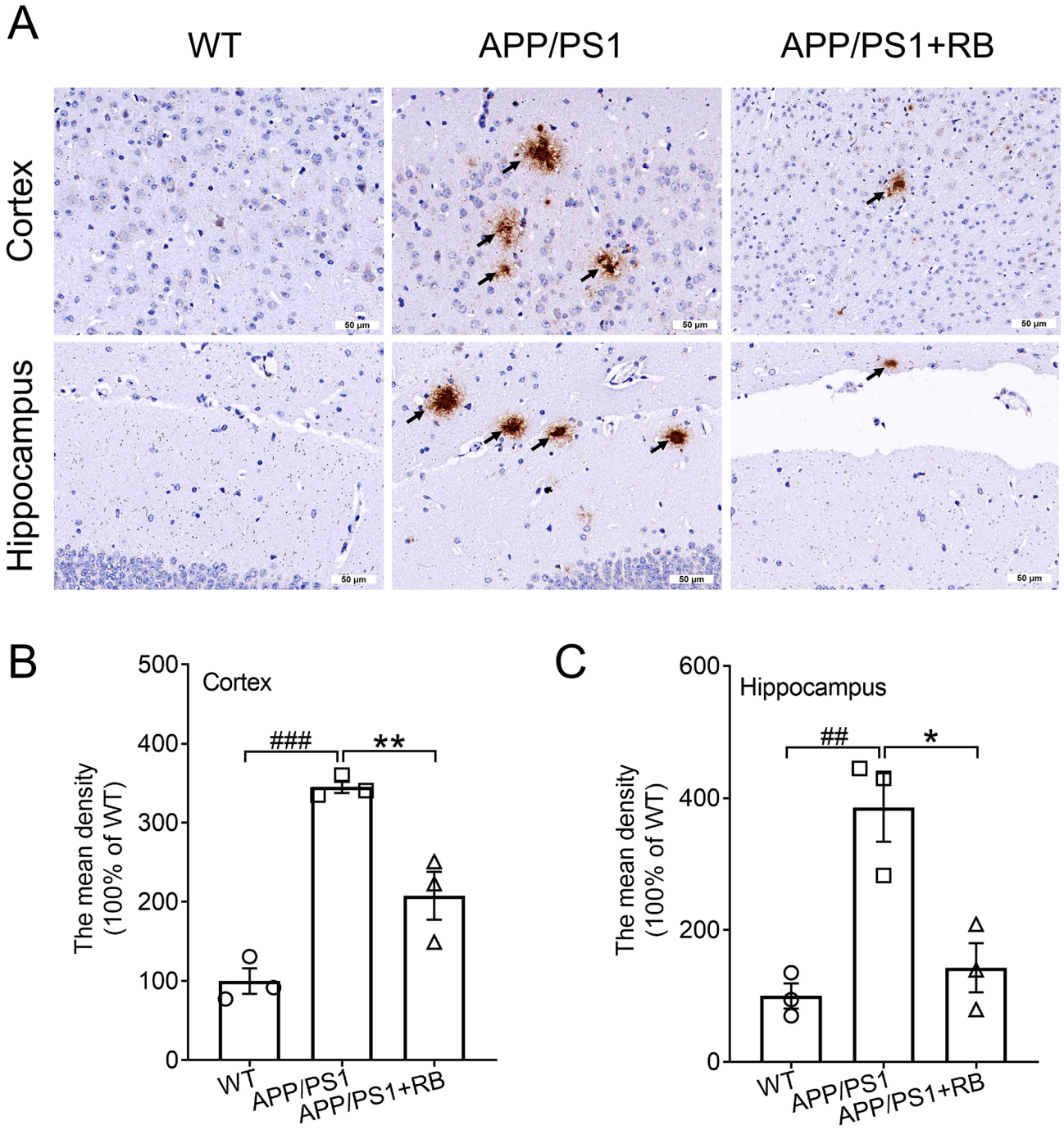

Fig. 2. RB inhibited deposition of Aβ plaques in the brains of APP/PS1 mice. Example images showing Aβ deposition in the (A) cortex and (C) hippocampus of APP/PS1 mice ($n = 3$). Scale bar is equal to 50 μm for 40× and 200× magnification, respectively. The arrows indicate the Aβ plaques in the cortex and hippocampus. Semi-quantitative analysis of Aβ deposition in the (B) cortex and (C) hippocampus of APP/PS1 mice, expressed as the fold change relative to the WT group ($n = 3$). Results were presented as means ± SEM. $^{\#\#}p < 0.01$ and $^{\#\#\#}p < 0.001$ compared with WT mice; $^{*}p < 0.05$ and $^{**}p < 0.01$ compared with APP/PS1 mice. SEM, standard error of the mean.

the expression levels of phosphorylated IKK, IκB, and NF-κB were all augmented ($p < 0.001$) (Fig. 5A–D). For all original WB figures in Fig. 5A, see the **Supplementary Material-original images of WB**. Both 5 μM and 20 μM RB, significantly inhibited the activation of IKK, IκB, and NF-κB ($p < 0.05$) (Fig. 5A–D). The red fluorescence–labeled NF-κB and the blue fluorescence–labeled nucleus overlapped much more in the Aβ_{1-42}-exposed N2a cells than in the CTRL N2a cells, a phenomenon that was finally reversed by RB treatment (Fig. 5E). Consequently,

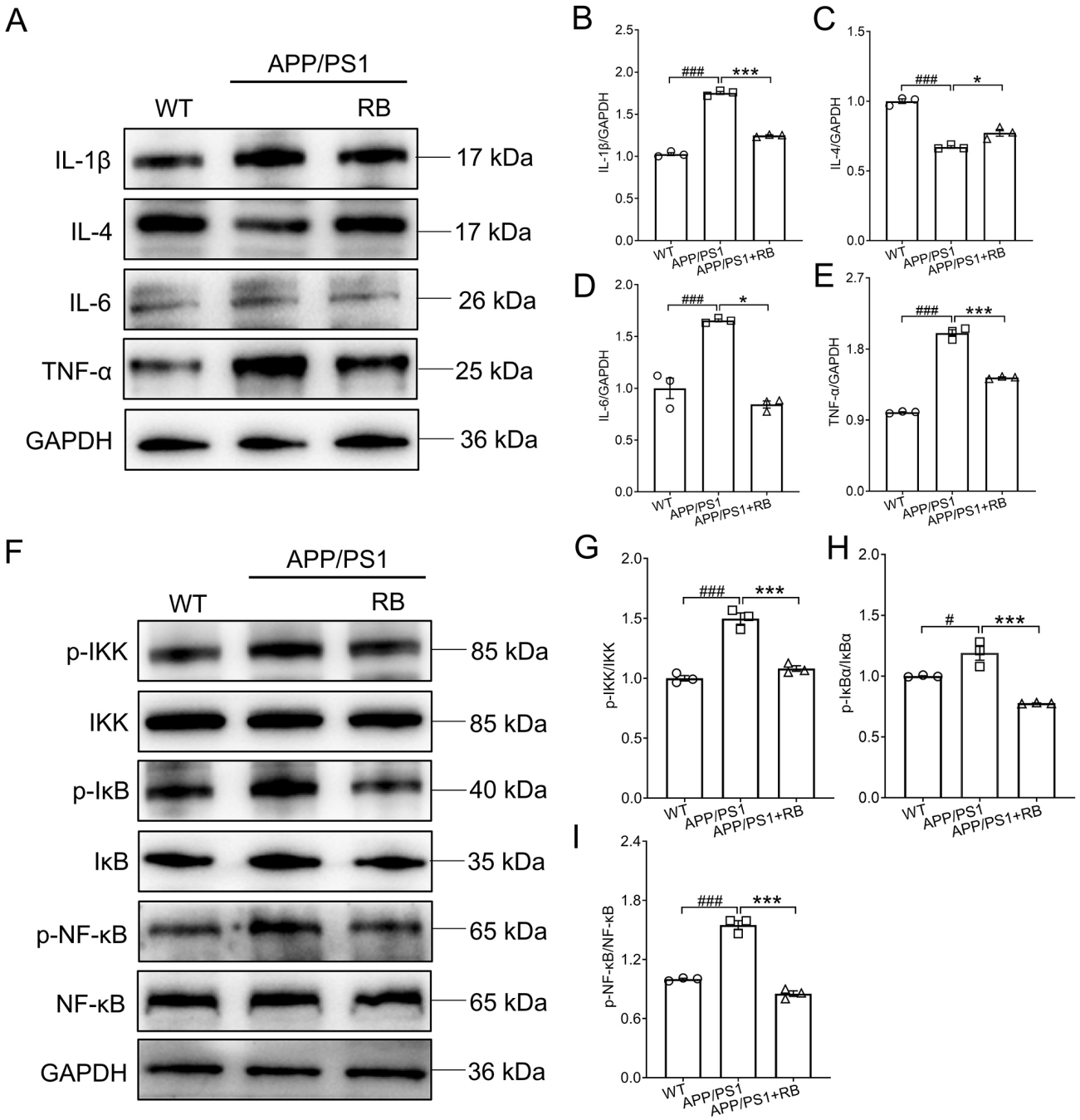

Fig. 3. RB suppressed neuroinflammation in the brains of APP/PS1 mice. (A) RB blocked the production of IL-1β, IL-6, and TNF-α and promoted that of IL-4 in the brains of APP/PS1 mice (n = 3). Semi-quantitative analysis of (B) IL-1β, (C) IL-4, (D) IL-6, and (E) TNF-α which was normalized to GAPDH and presented as the fold of the WT group (n = 3). (F) RB blunted the activation of IKK/IκB/NF-κB in the brains of APP/PS1 mice (n = 3). Semi-quantitative analysis of (G) p-IKK, (H) p-IκB, and (I) p-NF-κB which was normalized to their total proteins and presented as the fold of the WT group (n = 3). Results were presented as means ± SEM. $^{\#}p < 0.05$ and $^{\#\#\#}p < 0.001$ compared with WT mice; $^{*}p < 0.05$ and $^{***}p < 0.001$ compared with APP/PS1 mice. IKK, inhibitor of kappa B kinase; IκB, inhibitor of NF-κB; NF-κB, p-nuclear factor kappa-B.

these findings indicate that RB suppresses inflammation in Aβ_{1-42}-treated N2a cells, which may partially involve the IKK/IκB/NF-κB pathway (Fig. 5F).

4. Discussion

This study investigated the neuroprotective effects of RB on AD using *in vivo* and *in vitro* models. Memory deficits and learning dysfunction in the APP/PS1 mice were

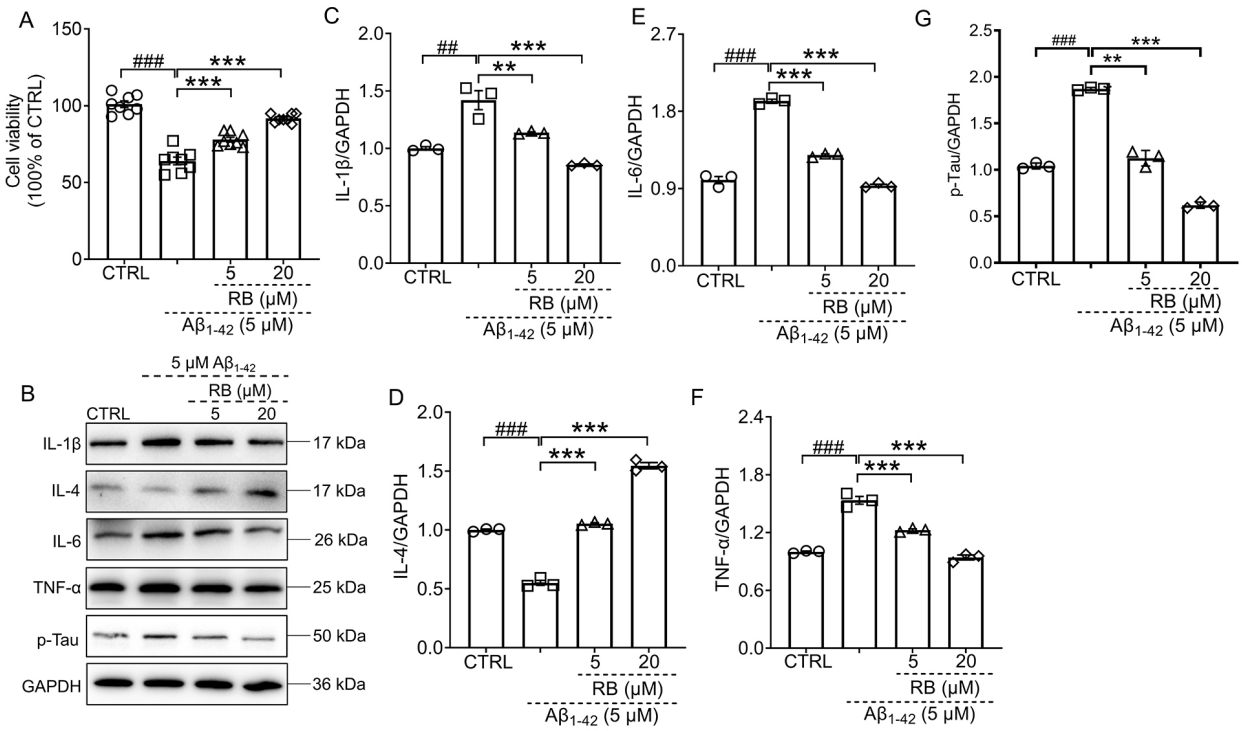

Fig. 4. RB protected N2a cells against A$\beta_{1–42}$-induced cell damage and inflammation. (A) RB improved cell viability of A$\beta_{1–42}$-induced N2a cells (n = 8). (B) RB suppressed the production of IL-1β, IL-6, TNF-α and p-Tau and increased that of IL-4 in the A$\beta_{1–42}$-exposed N2a cells (n = 3). Semi-quantitative analysis of (C) IL-1β, (D) IL-4, (E) IL-6, (F) TNF-α and (G) p-Tau was conducted, with expression levels normalized to GAPDH and expressed as fold change relative to the CTRL N2a group (n = 3). Results were presented as means ± SEM. $^{\#\#}p < 0.01$ and $^{\#\#\#}p < 0.001$ compared with CTRL N2a cells; $^{**}p < 0.01$ and $^{***}p < 0.001$ compared with A$\beta_{1–42}$-exposed N2a cells.

improved by RB on behavioral tests. RB treatment significantly inhibited the cerebral expression of Aβ through IHC analysis. Moreover, neuroinflammation was blunted in the brains of the RB-treated mice based on decreases in pro-inflammatory cytokines, increases in IL-4, and the inactivation of IKK/IκB/NF-κB. Subsequently, the efficacy of RB in reducing inflammation was further confirmed in N2a cells exposed to A$\beta_{1–42}$. RB treatment enhanced the viability of N2a cells exposed to A$\beta_{1–42}$, while also modulating the secretion of inflammatory cytokines and suppressing IKK/IκB/NF-κB pathway activation, as well as NF-κB nuclear transfer. These findings indicate that RB alleviates symptoms similar to those of AD, which may act by inhibiting neuroinflammation. Our study provides an experimental basis for future pharmacological studies of RB, thus facilitating the development of AD drugs from natural products.

Natural products have great potential for use in drug development. On one hand, they can be directly developed as new drugs to treat diseases. However, their novel and diverse structures make them lead compounds in the synthesis of more effective drugs [21]. The development of AD drugs has extensively explored natural products and their derivatives [13]. Emodin belongs to the anthraquinone family and inhibits the amyloidogenic pathway, NFT formation, neuroinflammation, and oxidative stress in AD-related cells and rodent models [22]. RB is also an anthraquinone compound whose antioxidant, anti-inflammatory, antidiabetic, and hepatoprotective effects have already been identified. RB is also a component of the traditional Chinese medicine Jia-Jian-Di-Huang-Yin-Zi decoction, which enhances behavioral performance and protects dopaminergic neurons from apoptosis in Parkinson's disease. Our study focused solely on the RB monomer as the subject of investigation. RB treatment significantly improved spatial memory in APP/PS1 mice, as evidenced by reduced escape latency during MWM navigation and increased target quadrant occupancy/crossings during probe trials. Non-spatial memory enhancements were observed through multiple behavioral measures: increased latency in step-down/step-through tests, reduced errors in passive avoidance, and elevated recognition indices in NOR. Pathologically, RB attenuated Aβ plaque deposition in AD-relevant brain regions. *In vitro* experiments confirmed RB protected N2a cells against A$\beta_{1–42}$-induced cytotoxicity, supporting its neuroprotective mechanism. These results indicated that RB relieves AD-like behavioral and pathological symptoms and serves as a neuroprotective factor in AD.

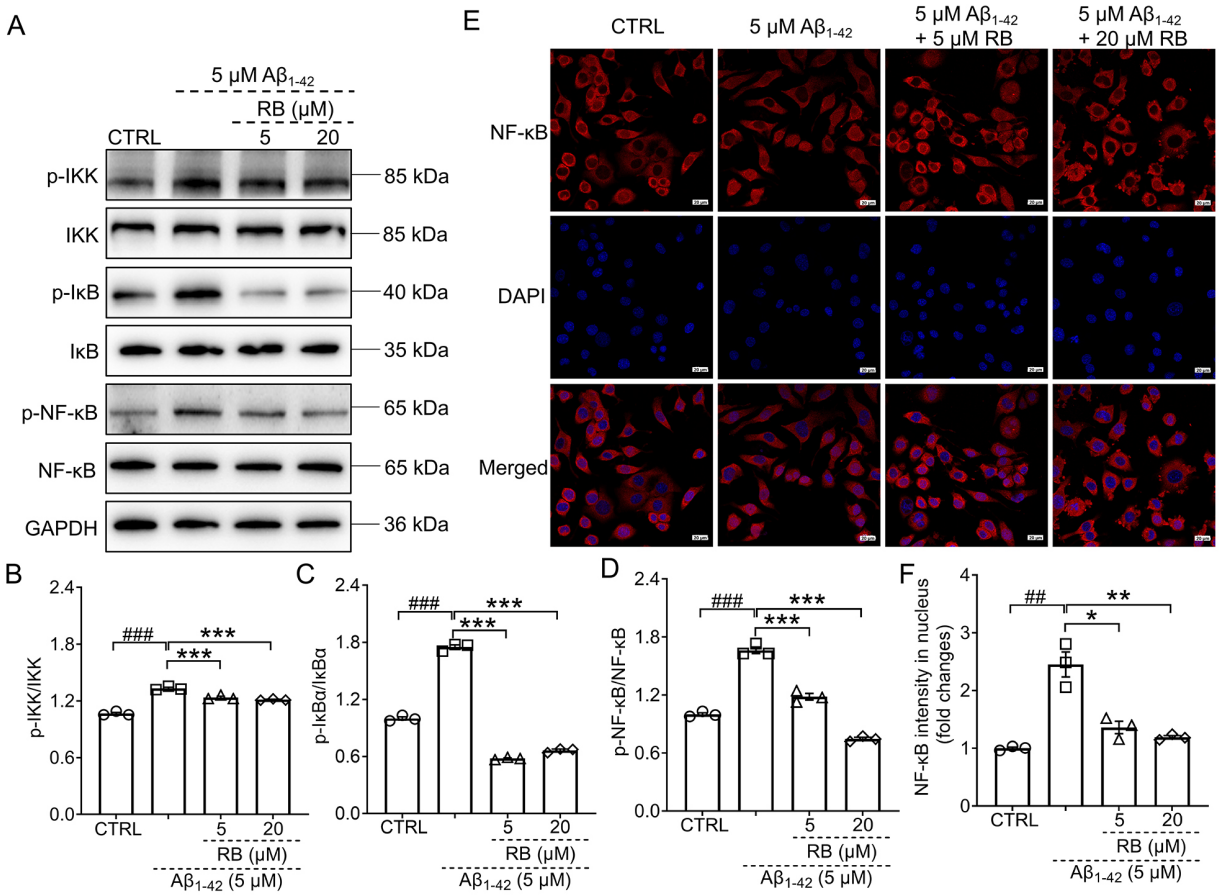

Fig. 5. RB inhibited the activation of IKK/IκB/NF-κB pathway in the Aβ$_{1–42}$-induced N2a cells. (A) RB down-regulated the phosphorylation of IKK, IκB, and NF-κB in the Aβ$_{1–42}$-treated N2a cells (n = 3). Semi-quantitative analysis of (B) p-IKK, (C) p-IκB, and (D) p-NF-κB which was normalized to their total proteins and presented as the fold of the control (CTRL) N2a group (n = 3). (E) RB prevented the nuclear translocation of NF-κB in N2a cells treated with Aβ$_{1–42}$ (n = 3). (F) The quantitative results of the nuclear fluorescence intensity of NF-κB were presented (n = 3). Scale bar is equal to 20 μm for 400× magnification. Results were presented as means ± SEM. $^{\#\#}p < 0.01$ and $^{\#\#\#}p < 0.001$ compared with CTRL N2a cells; $^{*}p < 0.05$, $^{**}p < 0.01$ and $^{***}p < 0.001$ compared with Aβ$_{1–42}$-exposed N2a cells.

Inflammatory cytokines play an important role in AD progression. Cerebral neuronal degeneration in AD is mainly caused by an increase in neuroinflammatory markers [23]. IL-1β accelerated the apoptosis of hippocampal neurons treated with Aβ$_{1–42}$ [24]. Caspase-1 blockade, a key upstream mediator of IL-1β processing, has been shown to mitigate cognitive deficits, amyloid-β deposition, and neuroinflammation in AD mouse models [25]. IL-6 is implicated in early amyloid plaque formation and specifically accumulates within cerebral plaques of AD patients [26]. This cytokine also promotes tau hyperphosphorylation in hippocampal neurons [27]. Clinically, plasma IL-6 levels correlate positively with brain inflammation and inversely with cognitive performance in AD patients [28]. Cerebral IL-6 signaling was further validated as a mediator of memory impairment in APP/PS1 mice [28]. Elevated TNF-α expression has been confirmed in both blood samples and postmortem brain tissues of AD patients [29]. After treating AD neurons with TNF-α, researchers detected the formation of abundant protein aggregates which were composed of Aβ and α-synuclein [30]. TNF-α and its receptor regulated neuronal necroptosis as confirmed both *in vitro* and *in vivo* [31]. In a phase II trial, Etanercept, a TNF-α inhibitor, demonstrated favorable safety in 20 AD patients but did not result in any significant changes in cognitive performance [32]. On the other hand, IL-4 overexpression in the brains of APP/PS1 mice improved AD pathogenesis including decreased Aβ deposition and gliosis and increased neurogenesis [33]. All of the above studies imply that it may be effective to alleviate AD by regulating inflammatory cytokines. In our study, RB reduced the expression levels of IL-1β, IL-6, and TNF-α while increasing the expression of IL-4 in both APP/PS1 mice and Aβ$_{1–42}$-induced N2a cells. These results indicate that the anti-AD effects of RB might be due to its capacity to reduce neuroinflammation.

As one of the best-studied pathways, NF-κB signaling is involved in neurodegenerative diseases [34]. For example, nuclear NF-κB regulated β-secretase expression at the transcriptional level, accelerating amyloid precursor protein processing and Aβ expression [35]. NF-κB signaling was also increased in reactive microglia and astrocytes to amplify the neuroinflammation and aggregate neurodegeneration [36]. Additionally, NF-κB also exerted its function through regulating apolipoprotein E activity, glutamate excitotoxicity, microRNA expression, and tau pathology [36]. Diverse natural products have demonstrated favorable pharmacological effects for regulating NF-κB in AD. Resveratrol was confirmed to suppress NF-κB and exert neuroprotection in Aβ_{25-35}-induced PC12 cells [37]. Accordingly, in APP/PS1 mice, RB markedly inhibited IKK, IκB, and NF-κB phosphorylation. RB also inactivated IKK/IκB/NF-κB pathway in Aβ_{1-42}-treated N2a cells on western blot and suppressed the nuclear translocation of NF-κB on an immunofluorescence analysis. These results were consistent with the inhibition of neuroinflammation. Therefore, RB attenuated AD pathogenesis, at least in part, by inhibiting neuroinflammation via the IKK/IκB/NF-κB pathway.

This study has several limitations. Only the expression profiles of inflammatory cytokines in APP/PS1 mouse brains were characterized. Neuroinflammation is primarily regulated by microglial and astrocytic activation [38]. Future studies will focus on quantifying microglial and astrocytic activation states in APP/PS1 mice to mechanistically validate RB's anti-inflammatory effects. On the other hand, based on the diverse pharmacological effects of RB in different disease models [16] and since AD is also a complex disease influenced by multiple factors, we will further explore whether RB has any biological activity other than anti-neuroinflammatory effects in AD models.

Here we discussed the results and how they compare to those of previous studies and working hypotheses. These findings and their significance should be considered in a wider context and explored more thoroughly in future studies.

5. Conclusions

This investigation represents the first comprehensive analysis of RB's therapeutic potential in AD. RB enhanced cognitive performance and reduced Aβ pathology in APP/PS1 mice, while also attenuating inflammatory responses and inhibiting NF-κB signaling in both *in vivo* and *in vitro* systems. Collectively, these data suggest RB mediates its protective effects through modulation of the IKK/IκB/NF-κB inflammatory signaling pathway.

Availability of Data and Materials

The original contributions presented in the study are included in the article, further inquiries can be directed to the corresponding author.

Author Contributions

YZZ, YZ and JF designed the research study. JF, SJN and JQP performed the research. YZ, SJN and WXG provided help on investigation and methodology. SJN and JQP operated software. YZ, JQP and WXG analyzed the data. YZ wrote the manuscript. YZZ and JF wrote review and editing. YZZ take charge of resources and funding acquisition. All authors contributed to editorial changes in the manuscript. All authors read and approved the final manuscript. All authors have participated sufficiently in the work and agreed to be accountable for all aspects of the work.

Ethics Approval and Consent to Participate

Animal experiments were conducted according to the guidelines of the Animal Ethics Committee of Jilin University (permit number: SY202103007) and under the supervision of the Jilin University Institutional Animal Care and Use Committee. All procedures were in accordance with ARRIVE guidelines.

Acknowledgment

Not applicable.

Funding

This research was funded by Natural Science Foundation of Jilin Province, China (20210101293JC).

Conflict of Interest

The authors declare no conflict of interest.

Supplementary Material

Supplementary material associated with this article can be found, in the online version, at https://doi.org/10.31083/JIN33497.

References

[1] Zhang XX, Tian Y, Wang ZT, Ma YH, Tan L, Yu JT. The Epidemiology of Alzheimer's Disease Modifiable Risk Factors and Prevention. The Journal of Prevention of Alzheimer's Disease. 2021; 8: 313–321. https://doi.org/10.14283/jpad.2021.15.

[2] Andronie-Cioara FL, Ardelean AI, Nistor-Cseppento CD, Jurcau A, Jurcau MC, Pascalau N, *et al*. Molecular Mechanisms of Neuroinflammation in Aging and Alzheimer's Disease Progression. International Journal of Molecular Sciences. 2023; 24: 1869. https://doi.org/10.3390/ijms24031869.

[3] Scheltens P, De Strooper B, Kivipelto M, Holstege H, Chételat G, Teunissen CE, *et al*. Alzheimer's disease. Lancet (London, England). 2021; 397: 1577–1590. https://doi.org/10.1016/S0140-6736(20)32205-4.

[4] Larkin HD. Lecanemab Gains FDA Approval for Early Alzheimer Disease. JAMA. 2023; 329: 363. https://doi.org/10.1001/jama.2022.24490.

[5] Si ZZ, Zou CJ, Mei X, Li XF, Luo H, Shen Y, *et al*. Targeting neuroinflammation in Alzheimer's disease: from mechanisms to clinical applications. Neural Regeneration Research. 2023; 18: 708–715. https://doi.org/10.4103/1673-5374.353484.

[6] Ni R. Positron Emission Tomography in Animal Models of Alzheimer's Disease Amyloidosis: Translational Implications. Pharmaceuticals (Basel, Switzerland). 2021; 14: 1179. https://doi.org/10.3390/ph14111179.

[7] Fan Z, Okello AA, Brooks DJ, Edison P. Longitudinal influence of microglial activation and amyloid on neuronal function in Alzheimer's disease. Brain: a Journal of Neurology. 2015; 138: 3685–3698. https://doi.org/10.1093/brain/awv288.

[8] Shen XN, Niu LD, Wang YJ, Cao XP, Liu Q, Tan L, *et al*. Inflammatory markers in Alzheimer's disease and mild cognitive impairment: a meta-analysis and systematic review of 170 studies. Journal of Neurology, Neurosurgery, and Psychiatry. 2019; 90: 590–598. https://doi.org/10.1136/jnnp-2018-319148.

[9] Princiotta Cariddi L, Mauri M, Cosentino M, Versino M, Marino F. Alzheimer's Disease: From Immune Homeostasis to Neuroinflammatory Condition. International Journal of Molecular Sciences. 2022; 23: 13008. https://doi.org/10.3390/ijms232113008.

[10] Thakur S, Dhapola R, Sarma P, Medhi B, Reddy DH. Neuroinflammation in Alzheimer's Disease: Current Progress in Molecular Signaling and Therapeutics. Inflammation. 2023; 46: 1–17. https://doi.org/10.1007/s10753-022-01721-1.

[11] Prins ND, Harrison JE, Chu HM, Blackburn K, Alam JJ, Scheltens P, *et al*. A phase 2 double-blind placebo-controlled 24-week treatment clinical study of the p38 alpha kinase inhibitor neflamapimod in mild Alzheimer's disease. Alzheimer's Research & Therapy. 2021; 13: 106. https://doi.org/10.1186/s13195-021-00843-2.

[12] Long HZ, Cheng Y, Zhou ZW, Luo HY, Wen DD, Gao LC. PI3K/AKT Signal Pathway: A Target of Natural Products in the Prevention and Treatment of Alzheimer's Disease and Parkinson's Disease. Frontiers in Pharmacology. 2021; 12: 648636. https://doi.org/10.3389/fphar.2021.648636.

[13] Liu JY, Guo HY, Quan ZS, Shen QK, Cui H, Li X. Research progress of natural products and their derivatives against Alzheimer's disease. Journal of Enzyme Inhibition and Medicinal Chemistry. 2023; 38: 2171026. https://doi.org/10.1080/14756366.2023.2171026.

[14] Wang NY, Li JN, Liu WL, Huang Q, Li WX, Tan YH, *et al*. Ferulic Acid Ameliorates Alzheimer's Disease-like Pathology and Repairs Cognitive Decline by Preventing Capillary Hypofunction in APP/PS1 Mice. Neurotherapeutics: the Journal of the American Society for Experimental NeuroTherapeutics. 2021; 18: 1064–1080. https://doi.org/10.1007/s13311-021-01024-7.

[15] Rao GMM, Rao CV, Pushpangadan P, Shirwaikar A. Hepatoprotective effects of rubiadin, a major constituent of Rubia cordifolia Linn. Journal of Ethnopharmacology. 2006; 103: 484–490. https://doi.org/10.1016/j.jep.2005.08.073.

[16] Watroly MN, Sekar M, Fuloria S, Gan SH, Jeyabalan S, Wu YS, *et al*. Chemistry, Biosynthesis, Physicochemical and Biological Properties of Rubiadin: A Promising Natural Anthraquinone for New Drug Discovery and Development. Drug Design, Development and Therapy. 2021; 15: 4527–4549. https://doi.org/10.2147/DDDT.S338548.

[17] Nasri S, Roghani M, Baluchnejadmojarad T, Balvardi M, Rabani T. Chronic cyanidin-3-glucoside administration improves short-term spatial recognition memory but not passive avoidance learning and memory in streptozotocin-diabetic rats. Phytotherapy Research: PTR. 2012; 26: 1205–1210. https://doi.org/10.1002/ptr.3702.

[18] Wan HL, Zhang BG, Chen C, Liu Q, Li T, He Y, *et al*. Recombinant human erythropoietin ameliorates cognitive dysfunction of APP/PS1 mice by attenuating neuron apoptosis via HSP90β. Signal Transduction and Targeted Therapy. 2022; 7: 149. https://doi.org/10.1038/s41392-022-00998-w.

[19] Wang C, Cai X, Wang R, Zhai S, Zhang Y, Hu W, *et al*. Neuroprotective effects of verbascoside against Alzheimer's disease via the relief of endoplasmic reticulum stress in Aβ-exposed U251 cells and APP/PS1 mice. Journal of Neuroinflammation. 2020; 17: 309. https://doi.org/10.1186/s12974-020-01976-1.

[20] Jiang Y, Li K, Li X, Xu L, Yang Z. Sodium butyrate ameliorates the impairment of synaptic plasticity by inhibiting the neuroinflammation in 5XFAD mice. Chemico-biological Interactions. 2021; 341: 109452. https://doi.org/10.1016/j.cbi.2021.109452.

[21] Newman DJ, Cragg GM. Natural Products as Sources of New Drugs over the Nearly Four Decades from 01/1981 to 09/2019. Journal of Natural Products. 2020; 83: 770–803. https://doi.org/10.1021/acs.jnatprod.9b01285.

[22] Mitra S, Anjum J, Muni M, Das R, Rauf A, Islam F, *et al*. Exploring the journey of emodin as a potential neuroprotective agent: Novel therapeutic insights with molecular mechanism of action. Biomedicine & Pharmacotherapy. 2022; 149: 112877. https://doi.org/10.1016/j.biopha.2022.112877.

[23] Kaur S, Bansal Y. Design, molecular Docking, synthesis and evaluation of xanthoxylin hybrids as dual inhibitors of IL-6 and acetylcholinesterase for Alzheimer's disease. Bioorganic Chemistry. 2022; 121: 105670. https://doi.org/10.1016/j.bioorg.2022.105670.

[24] Gu X, Wu H, Xie Y, Xu L, Liu X, Wang W. Caspase-1/IL-1β represses membrane transport of GluA1 by inhibiting the interaction between Stargazin and GluA1 in Alzheimer's disease. Molecular Medicine (Cambridge, Mass.). 2021; 27: 8. https://doi.org/10.1186/s10020-021-00273-8.

[25] Flores J, Noël A, Foveau B, Lynham J, Lecrux C, LeBlanc AC. Caspase-1 inhibition alleviates cognitive impairment and neuropathology in an Alzheimer's disease mouse model. Nature Communications. 2018; 9: 3916. https://doi.org/10.1038/s41467-018-06449-x.

[26] Huell M, Strauss S, Volk B, Berger M, Bauer J. Interleukin-6 is present in early stages of plaque formation and is restricted to the brains of Alzheimer's disease patients. Acta Neuropathologica. 1995; 89: 544–551. https://doi.org/10.1007/BF00571510.

[27] Quintanilla RA, Orellana DI, González-Billault C, Maccioni RB. Interleukin-6 induces Alzheimer-type phosphorylation of tau protein by deregulating the cdk5/p35 pathway. Experimental Cell Research. 2004; 295: 245–257. https://doi.org/10.1016/j.yexcr.2004.01.002.

[28] Lyra E Silva NM, Gonçalves RA, Pascoal TA, Lima-Filho RAS, Resende EDPF, Vieira ELM, *et al*. Pro-inflammatory interleukin-6 signaling links cognitive impairments and peripheral metabolic alterations in Alzheimer's disease. Translational Psychiatry. 2021; 11: 251. https://doi.org/10.1038/s41398-021-01349-z.

[29] Decourt B, Lahiri DK, Sabbagh MN. Targeting Tumor Necrosis Factor Alpha for Alzheimer's Disease. Current Alzheimer Research. 2017; 14: 412–425. https://doi.org/10.2174/1567205013666160930110551.

[30] Whiten DR, Brownjohn PW, Moore S, De S, Strano A, Zuo Y, *et al*. Tumour necrosis factor induces increased production of extracellular amyloid-β- and α-synuclein-containing aggregates by human Alzheimer's disease neurons. Brain Communications. 2020; 2: fcaa146. https://doi.org/10.1093/braincomms/fcaa146.

[31] Xu C, Wu J, Wu Y, Ren Z, Yao Y, Chen G, *et al*. TNF-α-dependent neuronal necroptosis regulated in Alzheimer's disease by coordination of RIPK1-p62 complex with autophagic UVRAG. Theranostics. 2021; 11: 9452–9469. https://doi.org/10.7150/thno.62376.

[32] Butchart J, Brook L, Hopkins V, Teeling J, Püntener U, Culliford D, *et al*. Etanercept in Alzheimer disease: A randomized, placebo-controlled, double-blind, phase 2 trial. Neurology. 2015; 84: 2161–2168. https://doi.org/10.1212/WNL.0000000000001617.

[33] Kiyota T, Okuyama S, Swan RJ, Jacobsen MT, Gendelman HE, Ikezu T. CNS expression of anti-inflammatory cytokine interleukin-4 attenuates Alzheimer's disease-like pathogenesis in APP+PS1 bigenic mice. FASEB Journal: Official Publication of the Federation of American Societies for Experimental Biology. 2010; 24: 3093–3102. https://doi.org/10.1096/fj.10-155317.

[34] Camandola S, Mattson MP. NF-kappa B as a therapeutic target in neurodegenerative diseases. Expert Opinion on Therapeutic Targets. 2007; 11: 123–132. https://doi.org/10.1517/14728222.11.2.123.

[35] Chen CH, Zhou W, Liu S, Deng Y, Cai F, Tone M, *et al*. Increased NF-κB signalling up-regulates BACE1 expression and its therapeutic potential in Alzheimer's disease. The International Journal of Neuropsychopharmacology. 2012; 15: 77–90. https://doi.org/10.1017/S1461145711000149.

[36] Sun E, Motolani A, Campos L, Lu T. The Pivotal Role of NF-kB in the Pathogenesis and Therapeutics of Alzheimer's Disease. International Journal of Molecular Sciences. 2022; 23: 8972. https://doi.org/10.3390/ijms23168972.

[37] Yan Y, Yang H, Xie Y, Ding Y, Kong D, Yu H. Research Progress on Alzheimer's Disease and Resveratrol. Neurochemical Research. 2020; 45: 989–1006. https://doi.org/10.1007/s11064-020-03007-0.

[38] Oh E, Kang JH, Jo KW, Shin WS, Jeong YH, Kang B, *et al*. Synthetic PPAR Agonist DTMB Alleviates Alzheimer's Disease Pathology by Inhibition of Chronic Microglial Inflammation in 5xFAD Mice. Neurotherapeutics: the Journal of the American Society for Experimental NeuroTherapeutics. 2022; 19: 1546–1565. https://doi.org/10.1007/s13311-022-01275-y.